충격 댐퍼의 동특성과 가속 질량추가 현상에 대한 연구

Dynamic Behaviors of the Impact Damper and the Accelerated Mass Loading

왕 세명† ·박 종찬*

Semyung Wang and Jongchan Park

ABSTRACT

Dynamic behaviors of the impact damper are studied experimentally and numerically. In order to investigate wide range of excitation frequencies and amplitudes, a simple but high amplifying and bias-free experimental setup is designed. Experiments focused on the harsh operation condition demonstrate *Accelerated mass loading* which not only deteriorates the performance of the impact damper but also involves the structural resonance which should be avoided for the stability of the system. In the previous studies, instability or deterioration of the performance was reported for the off resonance frequency region. But this paper shows that the performance deterioration and structural resonances can be predicted. Using finite element modeling and analysis, accurate system parameters were derived and used for the numerical modeling employing the conservation of the momentum. Numerical study of the transient responses using 4th-order Runge-Kutta method demonstrates general performance of the system, and shows that *accelerated mass loading* phenomenon is deeply related with the vibration amplitudes and the mass of the auxiliary system.

1. Introduction

An impact damping which makes use of the momentum transfers between the primary system and auxiliary mass during the collision to reduce severe vibrations of the primary system is one method of passive vibration control. A single unit impact damper or just impact damper uses an auxiliary mass enclosed within a container or a cavity inside the primary system. Dynamic analysis and performance of the impact damper [1] have long been studied. Most of the previous investigators focused on the parameter study of the optimum performance at the original resonant frequency. Only some investigators studied how impact dampers perform over a wide range of excitation frequencies and amplitudes. Popplewell et al. [2] reported in their forced vibration experiments that excitation frequencies at lower than the natural frequency produce negative damping, which case the structure vibrates more than without the impact damper. Along with the optimum performance, avoiding resonance is an important issue for a practical point of view. But, there has been little research about the resonance of the impact damper. Thus, the main emphasis of this paper is cast on resonant characteristics of the impact damper. Experimentally and numerically, this paper will show that resonances of an impact damper have non-linear characteristics with respect to the phase of the impact.

† 왕 세명; 광주과학기술원 기전과
E-mail : smwang@gist.ac.kr
Tel : (062)970-2390, Fax : (062) 970-2384
* 광주과학기술원

2. Physical model and experimental set-up

The system of the impact damper consists of a cart fixed at the middle of a fixed-fixed circular beam and a freely moving mass located between two columns of the cart. The cart motion is confined to move in x direction only on x-y plane by a low-friction linear guider. The difference of the given experimental set-up to the previous studies [3-6] is the enforced motion excitation not a force excitation and its measurement through acceleration signals. Rigid clamping of the beam to the shaker makes it possible to impart a motion not a force. Transmissibility, the ratio of the cart displacement to that of the input is used to estimates the degree of damping throughout the paper. For the given system, force excitation with a soft spring was inadequate to impart a wide range of excitation amplitude to the cart, which has been used conventionally for the impartation of the excitation force. Another feature of the designed experimental set-up is bias-free motion of the primary mass. Biased motion is avoided by employing a fixed-

fixed beam because the direction of the cart motion is perpendicular to the beam axis and symmetric to the x-z plane regardless of its magnitude comparing to the end effect of cantilevered beam.

3. Numerical modeling of the impact system

For the numerical analysis, the impact damper is modeled with 2-d.o.f system with an equivalent linear stiffness k, effective mass of primary mass m_p, auxiliary mass m_a and viscous damping c as shown in figure 1.

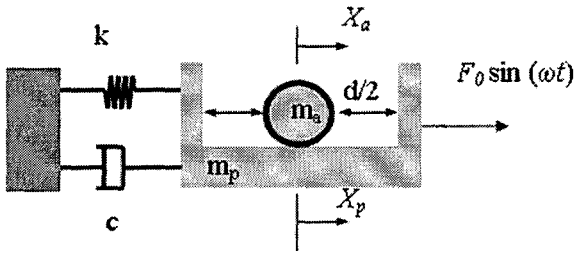

Figure 1- Two degree of freedom system model for a numerical analysis.

The equations of motion can be expressed as follows,

$$m_p\ddot{X}_p + c\dot{X}_p + kX_p = F_0 \sin(\omega t) \quad (1)$$

$$m_a\ddot{X}_a = 0 \quad (2)$$

where over-dots refer to the differentiation with respect to time and subscripts "a" and "p" represent physical values of primary and auxiliary masses, respectively.

Finite element analysis is utilized to calculate the equivalent linear stiffness of the beam. Calculated generalized mass of the primary mass is 1kg and generalized stiffness is 22848.94 N/m. 4.2% of modal damping from the experiment is used. And, 40% of the beam mass is added to the primary mass. 4th-order Runge-Kutta method is used for the numerical computation. Fast-Fourier transformed value of displacement of input and primary mass are used to represent the magnitude of vibration. For the correlation between the experimental results with an enforced motion and numerical simulation of the force input, the following relation between force and base motion (input displacement) is utilized.

$$F_0 = X_0\sqrt{k^2 - c^2\omega^2} \quad (3)$$

where X_0 is magnitude of the input displacement, ω is driving frequency in radian and F_0 is the magnitude of driving force.

Impacts between the primary mass and auxiliary mass are implemented by updating the state variables with calculated values after the impact. On the basis of the conservation of linear momentum and using the coefficient of restitution e, eq. (6), updated state variables can be calculated,

$$\dot{X}_p^+ = \frac{(1-\eta e)}{(1+\eta)}\dot{X}_p^- + \frac{\eta(1+e)}{(1+\eta)}\dot{X}_a^- \quad (4)$$

$$\dot{X}_a^+ = \frac{(1+e)}{(1+\eta)}\dot{X}_p^- + \frac{(\eta-e)}{(1+\eta)}\dot{X}_a^- \quad (5)$$

$$e = -\frac{(\dot{X}_p^+ - \dot{X}_a^+)}{(\dot{X}_p^- - \dot{X}_a^-)} \quad (6)$$

where η is mass ratio, m_a/m_p and the superscripts "+" and "-" represent the states just before and after the impact, respectively.

The most frequently used scheme of identifying the time of impact[1,3, 7-9] is checking the condition weather the relative displacement is less than a given criteria values or not, given as eq. (7).

$$R(|X_p(t_{n+1}) - X_a(t_{n+1})|) - d/2 \le R_c \quad (7)$$

$$R(|X_p(t_{n+1}) - X_a(t_{n+1})|) - d/2 \le 0 \quad (8)$$

where R refers to the relative location of the masses, d is clearance, R_c is a criterion value and sub-script in t refers to the number of analysis step.

The criterion of the previous research has been used on the condition that sufficiently small sampling time could reduce the error. However, when the relative position $R(t_n)$ at time step t_n is bigger than criterion, R_c, impact occurs at time step t_{n+1} as shown in figure 2 (a), which is negative collision.

Quantitatively, the error of the negative collision is negligibly small when the sampling time is sufficiently small. But, it can cause serious problem if it occurs when the velocity difference of the primary mass and auxiliary mass is small and mass ratio is considerably large. When the impact with small velocity difference occurs, the relative position after impact will remain within the criterion, R_c in the following step. This could provoke a continuous negative collision which means unreasonable additional energy loss. In order

to overcome those errors in the numerical analysis, improved scheme of identifying contact is developed. In this method, impact condition is checked whenever the relative position is less than half of the clearance given as eq. (8). With this condition, collision always occurs right after two masses pass behind each other. But, as shown in figure 2(b), state variables after impact are calculated with the state variables at time step t_n not at time step t_{n+1}. The consequence of the new criterion is the sustained motion of the auxiliary mass to avoid self-inducing repeated collision; any consecutively identified collision will trigger the sustained motion of the auxiliary mass by the primary mass. Sustained motion is more reasonable than self-inducing repeated collisions or negative collisions.

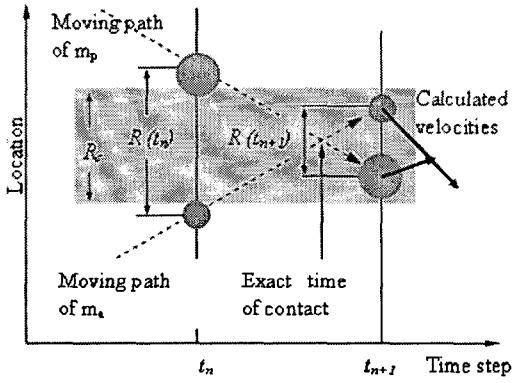

(a) Negative collision

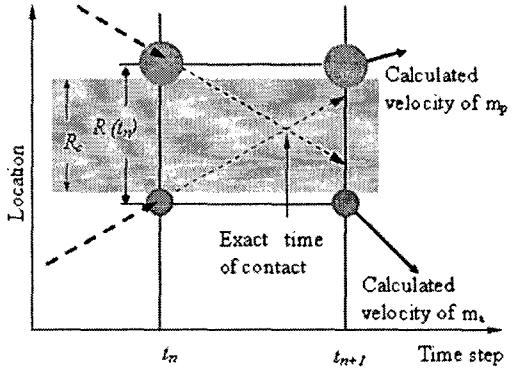

(b) Improved scheme

Figure 2- Numerical simulation trajectory of primary mass and auxiliary mass.

4. Dynamic behaviors of the impact damper

Figure 3 represents transmissibility diagrams of experiments and numerical simulation according to two test conditions listed in table 1 and the figure caption.

Table 1. Conditions for the experiments and numerical simulations represented in the figure 3 (d= 2.6mm, η=0.57).

Name	F_0	X_{0avg}(average value of the frequency sweep)
Exp_a		0.52 mm
Exp_b		0.97 mm
$Numr_a$	22 N	
$Numr_b$	12 N	

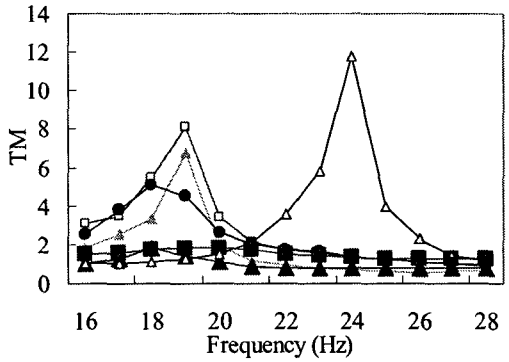

(a) Frequency response functions;△-experiments without auxiliary mass with X_{0avg} = 0.52mm; other conditions listed in Table 1, ▲-Exp_a; ▲-Exp_b; ■-$Numr_a$; □-$Numr_b$, ●-F_0=18 N.

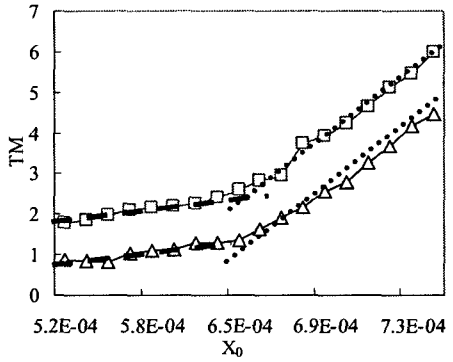

(b) Transmissibility with respect to the input displacement at 19Hz, △ -experiments, □ - numerical simulation.

Figure 3- Numerical simulation and experiment of the impact damper

Figure 3 shows interesting features that impact damper decreases the displacement of the primary mass drastically at the original resonance frequency, 24Hz and there is little negative effect for lower level input cases of Exp_a and $Numr_a$. However, for

higher input cases of Exp_b and $Numr_b$, there are conspicuous resonant peaks at shifted frequency of 19 Hz. Figure 3 (a) shows strong non-linearity of the transmissibility or damping capability of the impact damper according to the input amplitude. Transmissibility curves in figure 3(b) are measured and analyzed at 19Hz experimentally and numerically. In figure 3(b), two clearly distinguished slopes of the transmissibility according to the input amplitude are observed. In order to study those nonlinear characteristics according to the input amplitudes, time trajectories of the experiments and numerical simulations are studied as shown in figure 4 and figure 5.

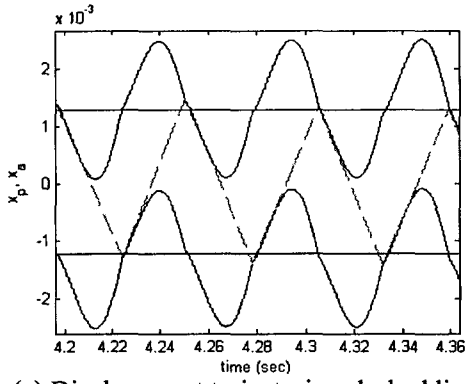

(a) Displacement trajectories: dashed line-auxiliary mass, solid line-primary mass.

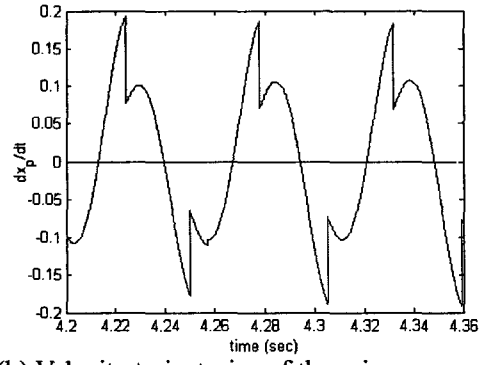

(b) Velocity trajectories of the primary mass.

Figure 4- Time trajectories of numerical simulation at 19Hz with 13 N input force (d= 2.6 mm, η=0.57):

In figure 4 (a), it is observed that dominant collisions take place evenly when the primary mass passes the equilibrium position which corresponds to the largest velocity of the primary mass as shown in figure 4 (b). And, velocities of the masses are out-of-phase each other. This configuration of impact affects the primary mass to transfer its momentum to the auxiliary mass with maximum loss. Figure 4 (b) shows abrupt reduction of the absolute value of the velocity after every impact, implying the loss of kinetic energy. This mechanism contributes to the low transmissibility or high damping in the first half of the input amplitude range in figure 3(b). Different kinds of collisions are illustrated in figure 5 according to the increasing displacement input.

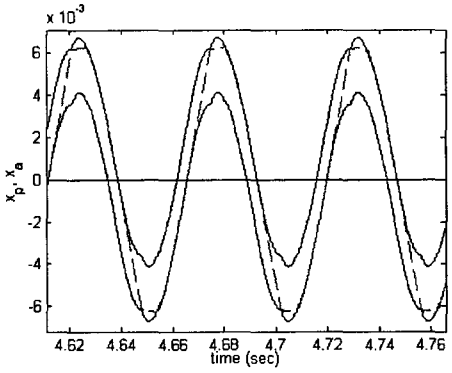

(a) Displacement (F_0= 18N)

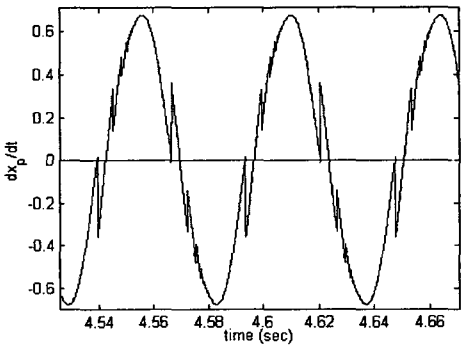

(b) Velocity (F_0=18N)

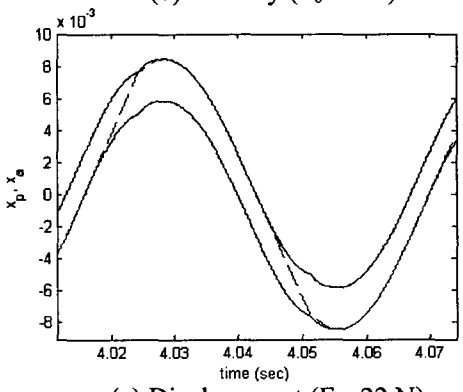

(c) Displacement (F_0=22 N)

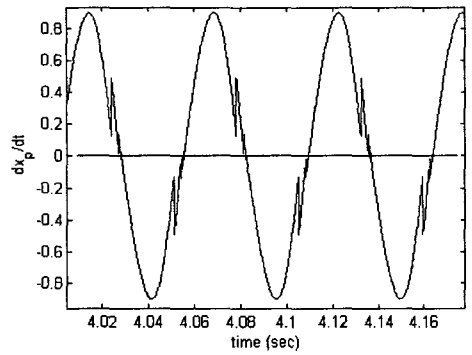

(d) Velocity (F_0= 22 N)

Figure 5- Time trajectories of numerical simulations, dashed line-auxiliary mass; solid line-primary mass.

In figure 5 (a) and (b), it is observed that dominant collisions take place regularly around the maximum strokes of the displacement and zero velocity of the primary mass resulting in less efficient momentum transfer to the contrary of the high damping in figure 3(b). Figure 5 (c) demonstrates that the collisions take place with the same direction of both masses. This kind of momentum transfer not only magnifies the amplitude of the primary mass but also adds kinetic energy of the auxiliary mass to the primary mass without modifying the original system resulting in the change of resonant frequency of the system. Numerical simulations of figure 4 and 5 are corroborated with experimental data. Figure 6 illustrates measured acceleration signals and magnitude scaled velocity of the primary mass. Velocity histories are achieved by integrating the acceleration signals. Then, the magnitudes are scaled to shows the time of impact because the measured acceleration signals are severely complex due to the high frequency structural vibrations caused by impact.

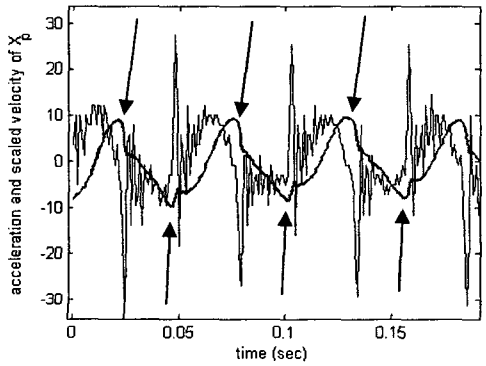

(a) 0.53mm input (F_0=13 N)

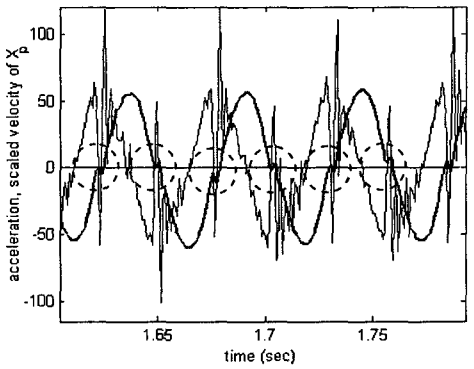

(b) 0.72mm input (F_0=18 N)

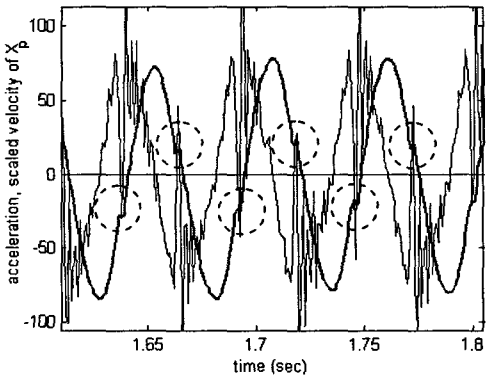

(c) 0.75 mm (F_0=22 N).

Figure 6- Experimental acceleration and scaled velocity at 19Hz, arrows indicate the time of impact in (a), dashed circles enclose the time of impact in (b) and (c) : — magnitude scaled velocity, — acceleration.

In figure 6, abrupt acceleration peaks imply the time of impact which shows good agreement with numerical simulations shown in figure 4 and 5.

It can be concluded that out-of-phase impact reduces the displacement of the primary mass with efficient momentum transfer. With increasing the input amplitude, the degree of damping changes following the configuration of the impact. In the limiting case, in-phase impact occurs resulting in mass loading effect through the kinetic energy influx into the primary mass, called as *accelerated mass loading* by the authors. In order to predict resonant shift quantitatively, *Rayleigh's energy method* of the system under harmonic motion is reflected. Numerical simulation of impact damper showed that the velocity of the primary mass and auxiliary mass can be regarded as the same when two masses collide with each other with the same direction, in-phase impact. Consequently, maximum displacement of the system is effected by the kinetic

energy influx through the impact.

For the system under consideration, *Rayleigh's energy equation* can be modified as eq. (9) on the condition that in-phase impact dominates the dynamics of the system, and the resulting resonant frequency, eq.(10), of the system under the kinetic energy influx by impacts is given,

$$T_{\max} = \frac{1}{2}(m_p + m_a)\dot{\chi}^2_{\max} = \frac{1}{2}k\chi^2_{\max} = U_{\max} \qquad (9)$$

$$\omega_{in} = \sqrt{\frac{k}{m_p + m_a}} \qquad (10)$$

where χ is the displacement of the primary mass resulting from the kinetic energy influx, and ω_{in} is resonant frequency of the impact induced mass loaded system. Numerical simulation and experiment of the impact damper with various mass ratios verify the validity of the eq. (9) and (10) on the condition of in-phase impact.

The implication of the experiments and numerical simulation is that freely moving mass undergoing periodic impacts can have mass effects into the system which causes resonance shift according to the phase of the impact, which is called *accelerated mass loading* by authors. For all the rigorous, the predicted resonant frequency of impact damper is corroborated with experiments and numerical simulations.

5. Conclusions

Dynamic responses of the impact damper have been investigated numerically and experimentally focused on the resonant vibration of it. Experiments of the horizontal impact damper showed the general performance and a shifted resonance of the integrated system. Time trajectories of the masses demonstrated that how the relative motion of the masse is related with the degree of damping. For a specific case, out-of-phase impact produces the most effective damping and the efficiency of the momentum transfer deteriorated with increasing input amplitudes which agrees with general theory. It is observed from the experiments and numerical simulation that the in-phase impact between masses induces kinetic energy influx into the primary mass with effective mass of the auxiliary mass resulting in mass loading effect even though the mass is freely moving under impacts. A simple prediction model for the accelerated mass loading effect is formulated on the basis of the observed condition.

References

[1] S. F. Masri, "General motion of impact damper", Journal of the Acoustical Society of America, **47**, 229-237 (1970).

[2] N. Popplewell, C. N. Bapat, K. McLachlan, "Stable periodic vibroimpacts of an oscillator", Journal of Sound and Vibration, **87**, 41-59 (1983).

[3] F. S. Collette, "A combined tuned absorber and pendulum impact damper under random excitation", Journal of Sound and Vibration, **216**, 199-213 (1998).

[4] S. E. Semercigil, F. Collette, D. Huynh, "Experiments with tuned absorber –impact damper combination", Journal of Sound and Vibration, **256**, 179-188 (2002).

[5] C. C. Cheng, J. Y. Wang, "Free vibration analysis of a resilient impact damper", International Journal of mechanical sciences, **45**, 589-604 (2003).

[6] K. Li, A. P. Darby, "An experimental investigation into the use of a buffered impact damper", Journal of Sound and Vibration, **291**, 844-860 (2006).

[7] C. N. Bapat, S. Sankar, "Single unit impact damper in free and forced vibration", Journal of sound and Vibration, **99**, 85-94 (1985).

[8] L. A. Chen, S. E. Semercigil, "A beam-like damper for attenuating transient vibrations of light structures", Journal of Sound and Vibration, **164**, (1993) 53-65.

[9] S. Ma, S. E. Semercigil, "A modified passive tuned absorber for secondary systems under random excitation", Journal of Sound and Vibration, **208**, (1997) 349-366